Bioactive Materials 32 (2024) 28–36

Contents lists available at ScienceDirect

Bioactive Materials

journal homepage: www.keaipublishing.com/en/journals/bioactive-materials

Chinese herb pollen derived micromotors as active oral drug delivery system for gastric ulcer treatment

Lijun Cai [a], Cheng Zhao [a], Xinyue Cao [a], Minhui Lu [a], Ning Li [a], Yuan Luo [b,**], Yongan Wang [b,***], Yuanjin Zhao [a,c,*]

[a] Department of Rheumatology and Immunology, Nanjing Drum Tower Hospital, School of Biological Science and Medical Engineering, Southeast University, Nanjing, 210096, China
[b] State Key Laboratory of Toxicology and Medical Countermeasures, Beijing Institute of Pharmacology and Toxicology, Beijing, 100850, China
[c] Southeast University Shenzhen Research Institute, Shenzhen, 518071, China

ARTICLE INFO

Keywords:
Micromotor
Chinese herb
Pollen
Drug delivery
Gastric ulcer
Wound healing

ABSTRACT

Considerable efforts have been devoted to treating gastric ulcers. Attempts in this field tend to develop drug delivery systems with prolonged gastric retention time. Herein, we develop novel Chinese herb pollen-derived micromotors as active oral drug delivery system for treating gastric ulcer. Such Chinese herb pollen-derived micromotors are simply produced by asymmetrically sputtering Mg layer onto one side of pollen grains. When exposed to gastric juice, the Mg layer can react with the hydrogen ions, resulting in intensive generation of hydrogen bubbles to propel the micromotors. Benefiting from the autonomous motion and unique spiny structure, our micromotors can move actively in the stomach and adhere to the surrounding tissues. Besides, their special architecture endows the micromotors with salient capacity of drug loading and releasing. Based on these features, we have demonstrated that our Chinese herb pollen-derived micromotors could effective deliver berberine hydrochloride and show desirable curative effect on the gastric ulcer model of mice. Therefore, these Chinese herb pollen-derived micromotors are anticipated to serve as promising oral drug delivery carriers for clinical applications.

1. Introduction

Gastric ulcer is one of the most common and tormented digestive diseases, which is characterized by gastric mucosa damages [1–3]. Significant scientific efforts have been placed on curing gastric ulcer [4–7]. Up to date, various drugs have been developed for gastric ulcer treatment in diverse formulations [8–12]. Among them, oral formulations stand out benefiting from their high gastric targeting, better patient compliance and low cost [13–16]. Based on oral formulations, drugs such as ranitidine, famotidine and omeprazole have been proven effective in promoting the recovery of gastric ulcer [17–19]. However, the curative effect of these oral formulations was greatly limited by the quick gastric emptying, which usually leads to short retention time. Although some particles have been devised to carry drugs to resist the quick gastric emptying, their retention time remains unsatisfactory due to the lack of structural design. Thus, insights regarding how to developing new drug delivery system with long gastric retention time may exert a profound impact on the treatment of gastric diseases.

In this paper, we proposed a novel Chinese herb pollen derived micromotors as active oral drug delivery system with prolonged retention time for gastric ulcer treatment, as schemed in Fig. 1. Chinese herb, which is an important branch of traditional Chinese medicine, has attacked worldwide scientific attention due to its multilevel functions [20–23]. Pollen grains as one of the most classic Chinese herbs not only exhibit desirable curative effect in regulating diseases, but also possess excellent adhesion due to their unique spiny architecture [24–27]. Besides, the hollow cavity inside pollens imparts them with excellent capacity for cargo loading, making them ideal as cargo carriers [28–31]. In

Peer review under responsibility of KeAi Communications Co., Ltd.
* Corresponding author. Department of Rheumatology and Immunology, Nanjing Drum Tower Hospital, School of Biological Science and Medical Engineering, Southeast University, Nanjing, 210096, China.
** Corresponding author.
*** Corresponding author.
E-mail addresses: luoyuan2006@163.com (Y. Luo), yonganw@126.com (Y. Wang), yjzhao@seu.edu.cn (Y. Zhao).

https://doi.org/10.1016/j.bioactmat.2023.09.009
Received 11 May 2023; Received in revised form 13 September 2023; Accepted 14 September 2023

contrast, micromotors are artificial self-propelled micro-devices that have come to the forefront as unique tools in many fields [32–34]. They can realize autonomous motion through energy transduction from external energy to kinetic energy [35,36]. Through specific design of propel mechanism, micromotors can even move actively *in vivo* [37–42]. Thus, it is conceived that the combination of pollen grains with micromotors can open new avenues for drug delivery.

Herein, we fabricated the desired Chinese herb pollen-derived micromotors by asymmetrically sputtering an Mg layer onto one side of sporopollenin exine capsules (SECs), which were collected from pollen grains of sunflowers. With this treatment, the SECs could move autonomously in the gastric juice due to the recoil force resulted from the generated H_2 bubbles. Benefiting from their autonomous motion and unique spiny structure, these pollen-derived micromotors could move spontaneously in the stomach and adhere to the surrounding tissues, thus prolonging the retention time and enhancing the bioavailability. Besides, the large surface-to-volume and the inner hollow cavity of SECs imparted these micromotors with excellent capacity of drug loading and releasing, making them serve as ideal carriers for drug delivery. As a proof of concept, these pollen-derived micromotors were loaded with berberine hydrochloride, an extract of Chinese herb coptis chinensis, to treat the gastric ulcer model of mice. Results showed that our pollen-derived micromotors exhibited desirable curative effect due to their active motion, excellent adherence, and good capacity of drug delivery, indicating great potential in oral drug delivery.

2. Results and discussion

In this experiment, the pollen grains were collected from sunflowers, which possessed spiny appendages (Fig. S1). As depicted in Fig. 2a, these pollen grains were composed of exine, intine and inner cells, with a layer of pollen cement covering on the surface. Scanning electron microscope (SEM) was applied to confirm their structure. As shown in Fig. S2, the original pollen grains exhibited a uniform size distribution of about 35 μm and possessed spiny structures around the surface. Besides, blocked porous structure was observed at the bottom of the spiny structure, which was ascribed to the covering of pollen cements (Fig. 2b). Aiming at making the pollens grains ideal as drug carriers, the pollens were then treated to remove the cements and biomolecules to dredge porous structure and get rid of the allergen according to the previous work [24]. As shown in Fig. 2a, the original pollen grains received sequential treatment of acetone and diethyl ether for defatting. Then, the potassium hydroxide was employed to remove the inner cells for obtaining the SECs. The SEM images of SECs showed that the porous structure was dredged (Fig. 2c). In addition, it's found that the size of SECs was bigger than the original pollen grains due to the alkaline lysis (Fig. S3). Overall, we obtained SECs with spiny and porous structure via defatting and chemical hydrolysis of the original pollen grains from sunflowers.

To fabricate the pollen-derived micromotors, the SECs were first dispersed on a slide (Fig. 3a). Then, a Mg layer was sputtered onto the surface of the slide with the help of ion sputtering instrument. After that, the slide received ultrasonic treatment to collect the pollen-derived micromotors. SEM was utilized to characterize the successful covering of Mg layer. As shown in Fig. 3b, one side of the SECs was covered with Mg layer while the other side maintained bare spiny morphology, indicating that the sputtering procedure had little damage on the architecture of SECs. Notably, the thickness of the Mg layer could be tailored by adjusting the sputtering time. Herein, we fabricated Mg-sputtered pollen-derived micromotors with thickness of 0.5 μm, 1.0 μm, 1.5 μm, and 2.0 μm. From the SEM images in Fig. S4, it's found that the pollens were coated with different thickness of Mg layer. Furthermore, energy-dispersive X-ray spectroscopy was employed to further confirm the asymmetry distribution of Mg layer (Fig. 3c and d). Results indicated that the amount of Mg elements on the Mg layer was much larger than that on the bare side. Also, energy-dispersive X-ray images of the pollen-derived micromotors were captured (Fig. S5). Mg elements were only observed on the half side coated with Mg layer. To summary, pollen-derived micromotors were prepared by sputtering a Mg layer onto one side of the SECs, which possessed desired asymmetry essential for autonomous movement.

The Mg layer on the micromotors could react with the H^+ in the biofluids, generating continual H_2. Due to the asymmetric distribution of the Mg layer, the H_2 bubbles were generated on one side of the micromotors. And the detachment of bubbles could lead to a counter-force for

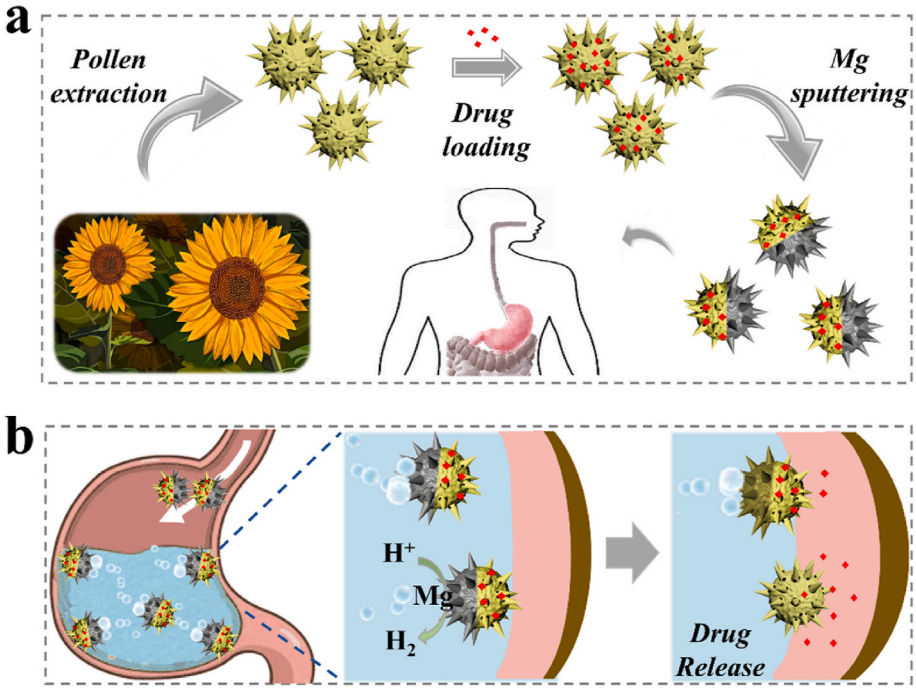

Fig. 1. Schematic illustration of Chinese herb pollen-derived micromotors as active oral drug delivery system for gastric disease treatment. (a) The fabrication process of Chinese herb pollen-derived micromotors. (b) The mechanism of pollen-derived micromotors working in the stomach.

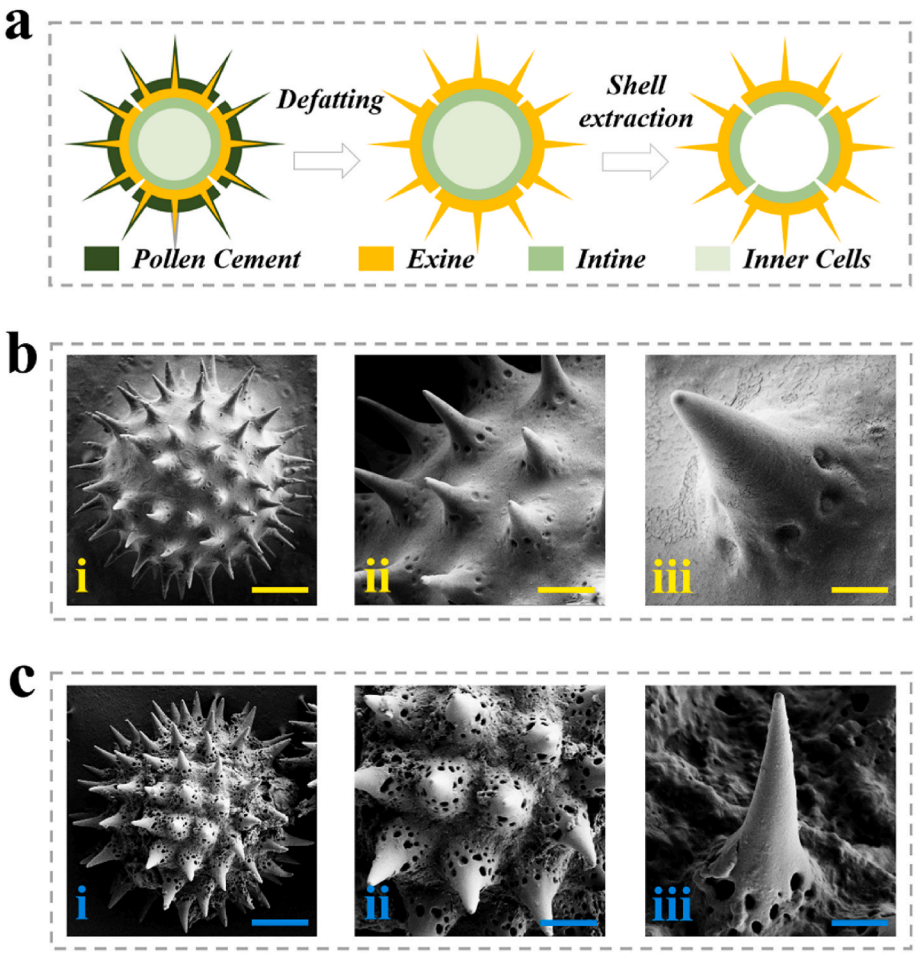

Fig. 2. Fabrication of SECs. (a) Scheme of generating SECs from pollen grains. (b) SEM images of pollen grains. Scale bars are 8 μm, 2.5 μm and 0.85 μm in (i), (ii) and (iii), respectively. (c) SEM images of SECs. Scale bars are 7.5 μm, 3.2 μm and 1.5 μm in (i), (ii) and (iii), respectively.

propelling the micromotors towards the opposite direction (Fig. 4a). We then exposed these pollen-derived micromotors to the artificial gastric juice to validate their capacity of autonomous movement. The motion routine was captured in time lapsing sequence, as shown in Fig. 4b and Movie S1. Results showed that our pollen-derived micromotors could realize self-propulsion in the artificial gastric juice benefiting from the continuous generation of bubbles. Besides, it's found that the motion performance including the velocity and lifetime of micromotors were related to the pH value of the surrounding fluids. Considering the acidic environment (pH 1–2) in the stomach [43,44], we recorded the lifetime and average velocity of the pollen-derived micromotors with different Mg thickness in stimulated gastric juice with different pH value. As recorded in Fig. 4c, the average velocity of micromotors declined with the increasement of pH value, which was because the generation of bubbles decreased with decreasing H^+ concentration. Also, thicker Mg layer contributed to higher average velocity. Furthermore, lower pH value of the surrounding fluids also contributed to longer lifetimes due to the slower reaction rate (Fig. 4d). To test the stability of these micromotors, we recorded the motion performance of the micromotors stored for 1 week. Results showed that the micromotors stored in a vacuum environment for one week exhibit similar motion performance with the initial micromotors, indicating good stability (Fig. S6). To sum up, our pollen-derived micromotors could realize self-propelled movement on account of Mg/H^+ reaction.

Supplementary video related to this article can be found at https://doi.org/10.1016/j.bioactmat.2023.09.009

In view of their unique spiny morphology and outstanding capacity of autonomous motion, these pollen-derived micromotors were speculated to act as active carriers which could move spontaneously and adhere to the surrounding tissues, thus resulting in a prolonged retention time. To verify these, we first evaluated the adhesive ability of SECs on the tissue surface by comparing the adhesive situation of SECs with that of spherical particles *in vitro*. To be specific, equivalent SECs and spherical particles were arranged to flow across the tissue surface. After that, phosphate buffered saline (PBS) flow was utilized to flush across the surface. Notably, red dyes were used to visualize the SECs. Optical images of the resultant tissue surface showed that the more SECs remained on the surface after the initial flow in comparison with spherical particles (Fig. S7a). After the PBS flushing, most spherical particles were flushed away while most SECs remained on the surface. Furthermore, we counted the particles remained on the surface to calculate retention rate (Fig. S7b). Results showed that near 75% SECs adhered to the tissue surface after the initial flow and less than 10% was flushed away by the PBS flow. In contrast, only 15% spherical particles left after the PBS flushing. These results indicated that SECs exhibited better adhesive ability due to their unique spiny structure, which could be ascribed to the lager contact area.

Then, we carried out an *in vivo* experiment to compare the retention situation of spherical particles, SECs and pollen-derived micromotors. Mice were grouped at random and received gavage of the three kinds of particles, respectively. Notably, gavage could prevent the micromotors from contact with other digestive tract parts. All the particles were dyed with fluorescent dyes. Then, mice were sacrificed at specific time points to take out their digestive tracts for analysis of particle retention. For the mice received gavage of spherical particles, fluorescence signal was observed in the lower digestive tract after 1 h and the fluorescence signal

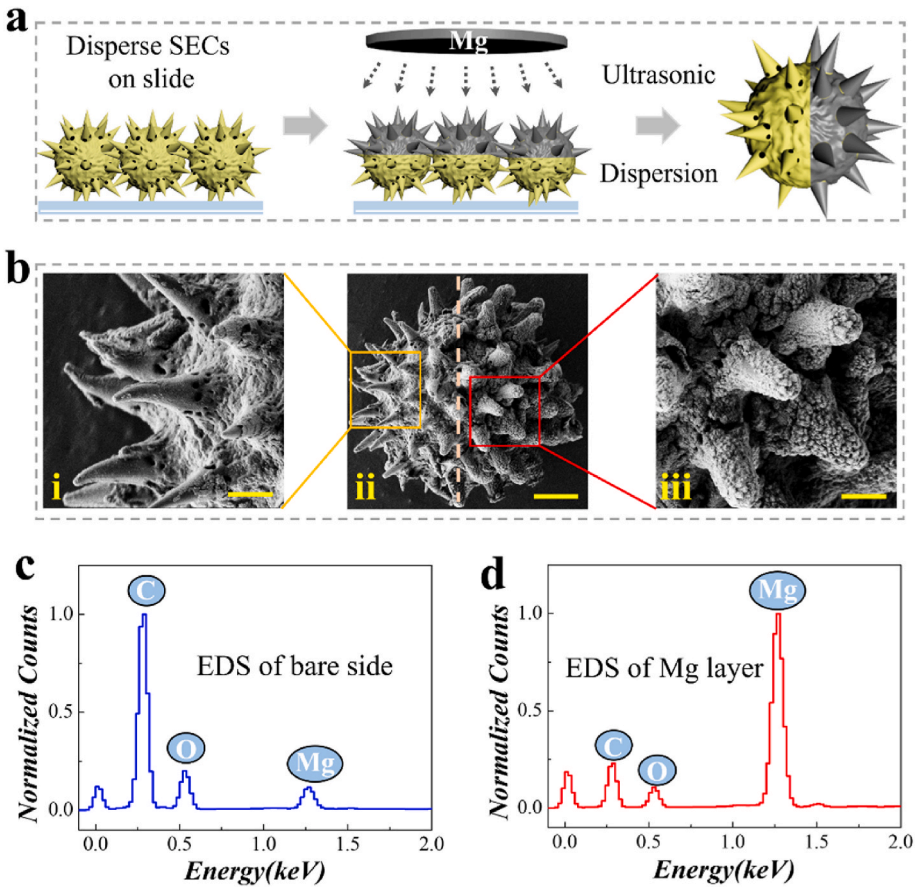

Fig. 3. Fabrication of pollen-derived micromotors. (a) Schematic illustration of fabricating pollen-derived micromotors. (b) SEM images of pure side of pollen-derived micromotor (i), the whole pollen-derived micromotors (ii) and the Mg layer side of pollen-derived micromotors (iii). Scale bars are 2 μm, 6 μm and 2 μm in (i), (ii) and (iii), respectively. (c–d) Energy-dispersive X-ray spectra of bare side (c) and Mg-coated side (d) of pollen-derived micromotor.

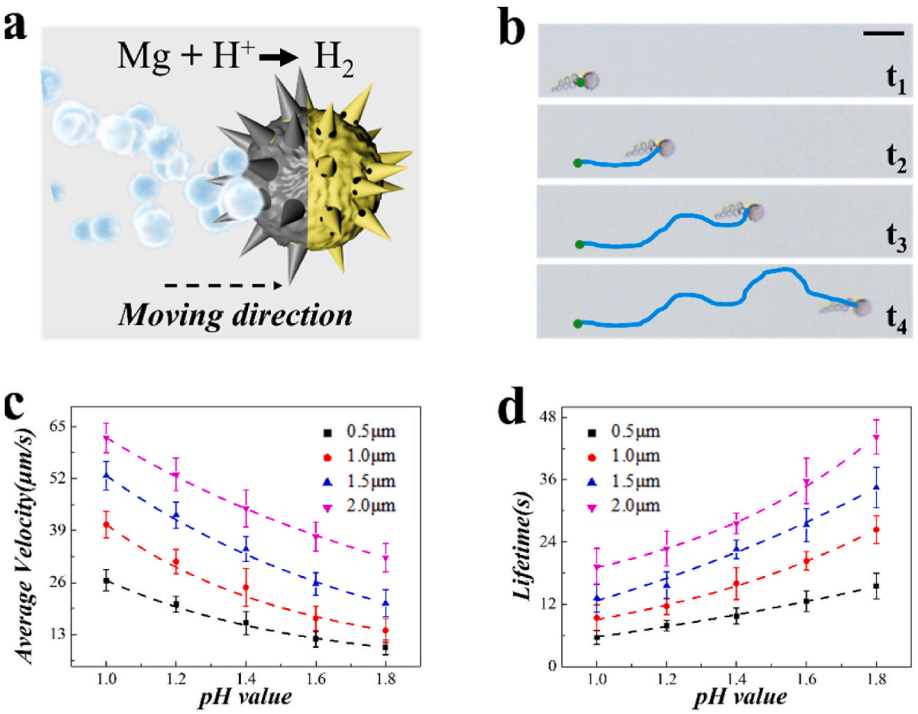

Fig. 4. Motion performance of pollen-derived micromotors. (a) Scheme of the autonomous motion mechanism. (b) Time-lapse sequence of pollen-derived micromotors' autonomous motion routine. Scale bar is 80 μm. (c) Statistical analysis of average velocity of pollen-derived micromotors with different Mg thickness in different pH value. (d) Statistical analysis of the lifetime of pollen-derived micromotors with different Mg thickness in different pH value.

decreased to a very low value after 3 h, indicating that the spherical particles were almost cleared out of the digestive tract with peristalsis (Fig. 5a). For the mice received gavage of SECs, fluorescence signal could be observed in the stomach after 3 h, which indicated that part of the SECs still stayed in stomach after 3 h and part of them were emptied from the stomach and entered the lower gastrointestinal tract (Fig. 5b). These results further proved that SECs exhibited better adhesive capacity than traditional spherical particles benefiting from their unique spiny architecture. For the mice received gavage of pollen-derived micromotors, after 1 h, strong fluorescence signal was detected in the stomach while little fluorescence signal was observed in the other parts of the digestive tract (Fig. 5c). Furthermore, even after 6 h, the stomach still exhibited strong fluorescence signal, indicating that our pollen-derived micromotors presented a longer retention time in the stomach. This was because that the pollen-derived micromotors could move spontaneously in the gastric juice. Notably, apart from the motion propelled by the bubble generation, the pollen-derived micromotors could move spontaneously towards the stomach wall as both micromotors and stomach wall are hydrophilic [14,45]. With the autonomous movement, the pollen-derived micromotors could move towards the tissue, which benefited the adherence to the tissue. Therefore, our pollen-derived micromotors could serve as active carriers with prolonged retention time benefiting from their spiny structure and autonomous motion.

We then demonstrated the drug delivery capacity of pollen-derived micromotors by employing Rhodamine B (RhB) as drug model through an *in vitro* experiment. RhB molecules could be loaded into SECs by soaking the SECs in the RhB aqueous solution, followed with vacuum treating. The RhB drug loading efficiency was as shown in Fig. S8. It's worth mentioning that the vacuum treating helped the RhB molecules enter the inner cavity, which could enhance the loading efficiency. In addition, large surface-to-volume ratio of SECs also contributed to more adsorption of RhB. Then, the micromotors loaded with RhB were exposed to artificial gastric juice at 37 °C to investigate their drug release performance. As shown in Fig. 5d, the intensity of fluorescence, which derived from RhB, deceased gradually with time going on because of the continual release of RhB from the SECs. From the cumulative release profile, a burst release of RhB was observed at the first 12 h and the cumulative release rate gradually increased and reached about 60% after 60 h (Fig. 5e). Besides, hemolysis test and biocompatibility test were carried out to validate the biosafety of our pollen-derived micromotors. Little difference was observed between the control groups and experimental groups, demonstrating the ideal biosafety of pollen-derived micromotors (Fig. S9 and Fig. S10). Thus, our pollen-derived micromotors presented excellent drug loading capacity and desirable drug release profile, acting as ideal carriers for drug release.

The unique self-propulsion, outstanding adhesive capacity and excellent drug delivery property made our pollen-derived micromotors ideal for active drug delivery. To test their practical capacity in curing diseases, we loaded these micromotors with berberine hydrochloride, an extract of Chinese herb coptis chinensis, to treat the gastric ulcer model

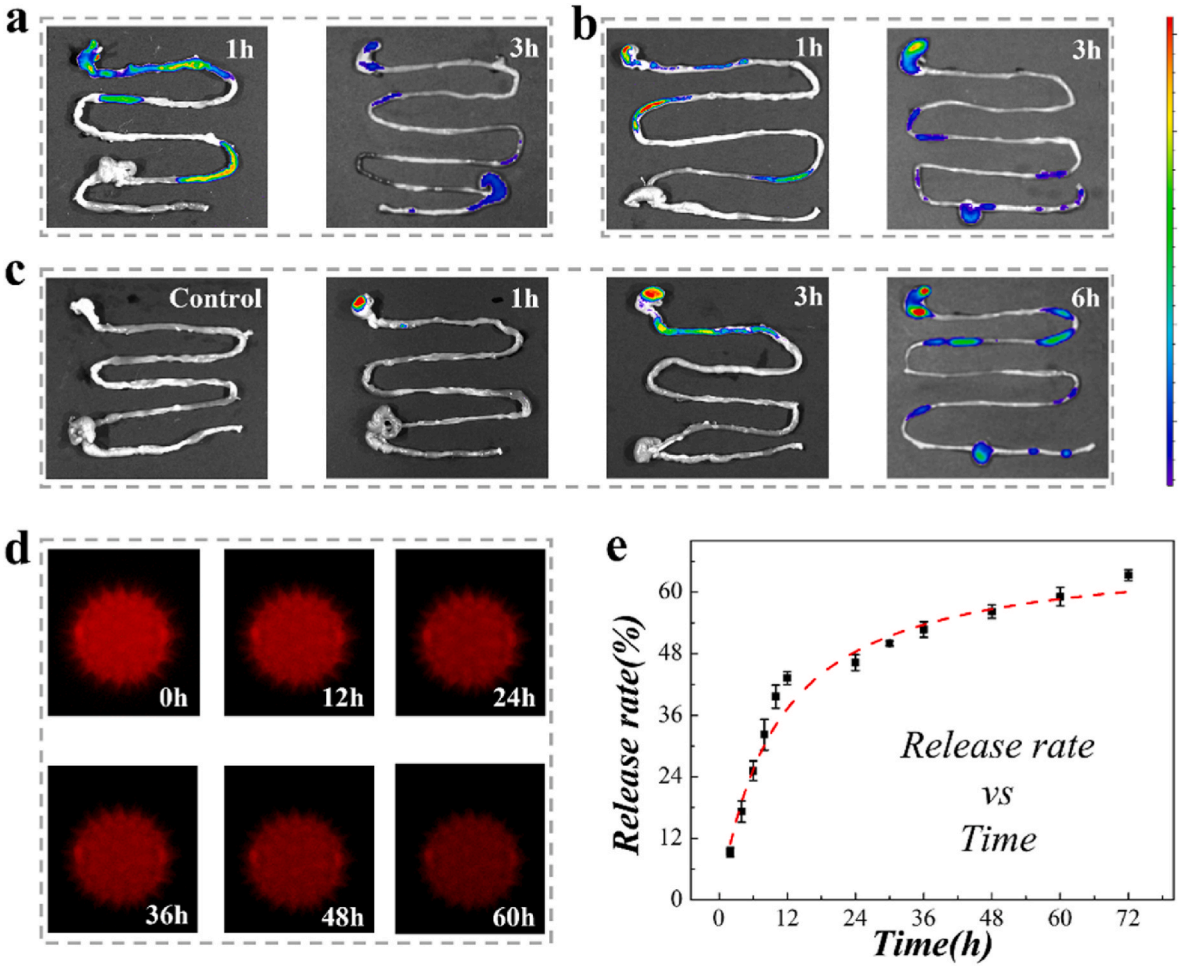

Fig. 5. Retention test *in vivo* and drug release *in vitro*. (a) The digestive tract of mice given gavage of spherical microparticles sacrificed at 1 and 3 h after gavage. (b) The digestive tract of mice given gavage of SECs sacrificed at 1 and 3 h after gavage. (c) The digestive tract of mice given gavage of spherical microparticles sacrificed at 0, 1, 3 and 6 h after gavage. (d) The time-lapse sequence fluorescence images of RhB-loaded SECs during drug release process. (e) The release kinetic profile of RhB-loaded SECs.

of mice. We first divided mice randomly into four groups. One of them was set as healthy group and the other three were induced to gastric ulcer by gavage of acetic acid at Day 0. We gave gavages to the healthy group with PBS and gave gavages to the other three diseased groups with PBS, free berberine hydrochloride and drug-loaded micromotors, respectively, on Day 1, Day 3, and Day 5. During the treatment, it's found that gastric ulcer affected the weight of mice, as shown in Fig. S11. To be specific, mice of healthy possessed gaining weights while mice with gastric ulcer started to lose weight from Day 1. Notably, weight of gastric ulcer-induced mice received gavage of PBS kept the downward trend. On the contrary, gastric ulcer-induced mice received gavage of free berberine hydrochloride maintained the same weight as Day 1 and started to gain weight gradually from Day 3. For the mice received gavage of drug-loaded micromotors, their weight kept an increasing trend from Day 1. These results indicated that our drug-loaded pollen-derived micromotors exhibited better curative effect than the free drugs, which could be ascribed to longer retention time.

To further evaluate the therapeutic efficacy, all the mice were sacrificed on Day 7 for histopathological analysis. The hematoxylin and eosin (HE) histology images were presented in Fig. 6a. HE results in healthy group showed that the mucosal layer structure was intact and the mucosal epithelial cells were normal without exfoliation. No edema or inflammatory cell infiltration were found in the mucosal layer. Besides, the gastric glands arranged orderly and tightly. By contrast, in the group of diseased mice received gavage of PBS, the tissue mucosa layer was damaged. To be specific, exfoliated epithelial cells, loose submucosal fibrous connective tissue, and massive inflammatory cell infiltration were observed. Furthermore, the arrangement of gastric glands was loose and large necrosis of gastric gland epithelial cells was observed. For those who received gavage of free berberine hydrochloride and drug-loaded micromotors, the mucosal damage was significantly improved. The group of drug-loaded micromotors exhibited rarer exfoliation of epithelial cells and slighter inflammatory cell infiltration than the group of free berberine hydrochloride. These results demonstrated that our drug-loaded pollen-derived micromotors exhibited better curative effect than the free drugs.

In view of that tumor necrosis factor (TNF-α) and interleukin-10 (IL-10) are involved in inflammatory regulation, their expression level in the tissues was assessed. As shown in Fig. 6b, a high-level expression of TNF-α was observed in the mice with gastric ulcer, which was because TNF-α plays a role in promoting inflammation. After the gavage of free berberine hydrochloride and drug-loaded micromotors, the expression of TNF-α decreased due to the relief of the symptoms. In addition, owing to excessive TNF-α and shortage of anti-inflammation of IL-10, the healing of gastric ulcer in the diseased mice was impeded. Notably, IL-10 can exhibit anti-inflammatory effect by reducing the expression of inflammatory factors including TNF-α. After the gavage of free berberine hydrochloride and drug-loaded micromotors, the expression of IL-10 increased (Fig. 6c). All these results implied that our pollen-derived micromotors served as efficient carriers for effective gastric ulcer treatment benefitting from their longer retention time and excellent capacity in drug delivery, indicating great potency in clinical medicine.

3. Conclusion

In summary, we have developed a novel kind of Chinese herb pollen-derived micromotors as an active oral drug delivery system for the treatment of gastric ulcer. The pollen-derived micromotors was produced by asymmetry sputtering a Mg layer onto one side of the SECs. After exposing to gastric juice, the Mg layer could react with H^+ to

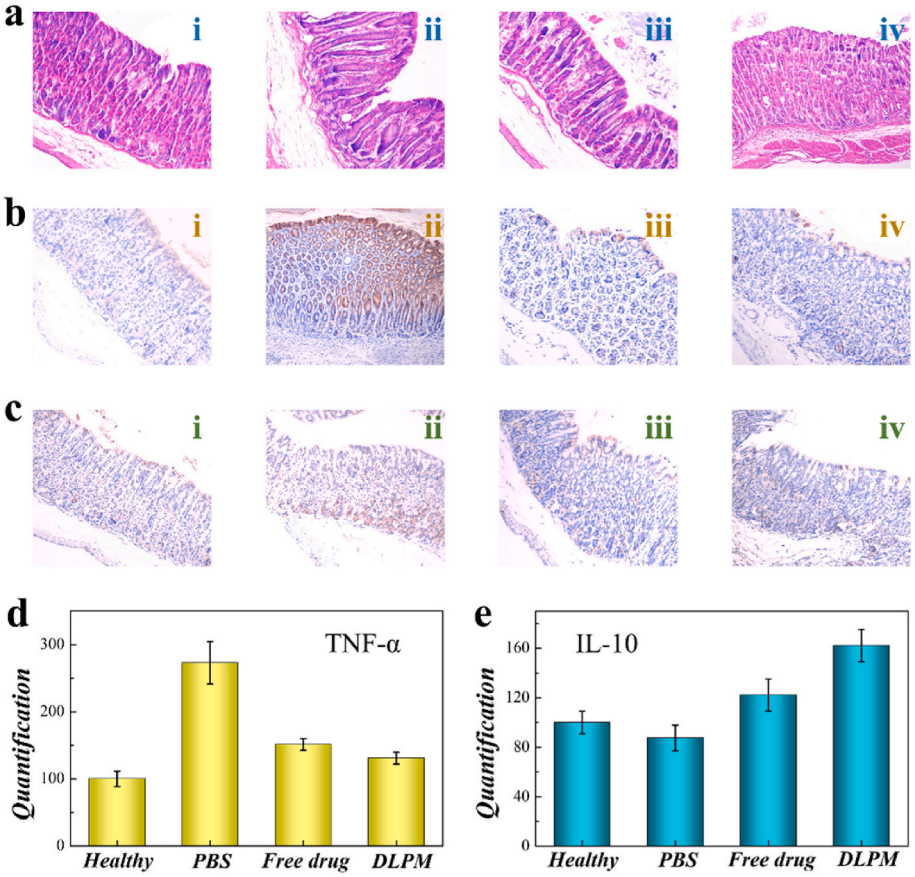

Fig. 6. Histopathological analysis. (a–c) Representative HE (a), TNF-***α*** (b) IL-10 (c), images of healthy mice (i), diseased mice received gavage of PBS (ii), free drug (iii), drug-loaded micromotors (iv). (d–e) Statistical analysis of expression quantification of TNF-***α*** (d) and IL-10 (e).

generate intensive bubbles to drive the micromotors to move. It's demonstrated that our micromotors could actively move in the stomach and adhere to surrounding tissues benefiting from their autonomous movement and unique spiny structure. In addition, their special structure endowed the pollen-derived micromotors with remarkable drug loading and release capabilities. Based on these characteristics, we proved that our micromotors could effectively move and adhere to deliver berberine hydrochloride, exhibiting an ideal therapeutic effect on mice gastric ulcer model. Thus, we envisioned that our novel Chinese herb pollen-derived micromotors could ushered in a new era for drug delivery.

4. Experimental section

4.1. Materials

The pollen grains were bought from Changhong Bee Industry Co., Ltd. The acetone, diethyl ether, ethanol, potassium hydroxide (KOH), and acetic acid were obtained from Sinopharm Chemical Reagent Co., Ltd. The Mg disk was purchased from Hefei Fangzun Metal Materials Co., Ltd. The artificial gastric juice was from Fuzhou Phygene Biotechnology Co., Ltd. The Rhodamine B and berberine hydrochloride were bought from BASF Chemical Co., Ltd and Macklin Biochemical Technology Co., Ltd, respectively. The phosphate buffer saline (PBS) and deionized (DI) water were self-prepared.

4.2. Fabrication of SECs

To fabricate the SECs, pollen grains of sunflowers were collected and immersed in water to wash away the large contaminating particulate matter, followed by natural air drying. Then, acetone (400 mL) was employed to soak the pollen grains (200 g) with stirring (300 rpm) at 50 °C for 3 h. After removing the acetone, deionized water (1 L, 50 °C) was added to the pollen grains under stirring (220 rpm) for 1 h. Next, the pollen grains were collected by vacuum filtration. The acetone treating procedure was repeated once. After air drying overnight, resultant pollen grains (20 g) were dispersed in diethyl ether (250 mL) and the mixture was kept stirring for 2 h (25 °C, 400 rpm). Defatted pollen grains were obtained by repeating the diethyl ether treating procedure for 3 times with processing time of 4 h, 8 h and 12 h, respectively. After that, the resultant pollen grains were collected by vacuum filtration. To remove the inner cytoplasm, 10% KOH (40 mL) was employed to soak the defatted pollen grains under stirring (80 °C, 800 rpm, 2 h). The KOH treating procedure was repeated for 5 times and each time the defatted pollen grains were collected via centrifugation at 6000*g* for 10 min. The SECs were finally obtained by vacuum filtrating the mixture.

4.3. Fabrication of pollen-derived micromotors

To fabricate the pollen-derived micromotors, the resultant SECs (0.1g) were dispersed in ethanol (5 mL) and the mixture was vortexed to uniform dispersion. After that, the mixture (100 μL) was transferred to a slide and spread evenly on a glass slide with the help of a scraper. With the volatilization of ethanol, SECs remained on the slide. Then, the slide with pollens were treated with plasma to make the pollens hydrophilic. Subsequently, the slide was put on the stage of ion sputtering instrument installed with a Mg disk, followed by Mg sputtering. Notably, the thickness of the Mg layer could be tailored by adjusting the sputtering time. Herein, we fabricated Mg-sputtered pollen-derived micromotors with thickness of 0.5 μm, 1.0 μm, 1.5 μm, and 2.0 μm. Next, the slide was immersed in ethanol and received ultrasonic treatment for 1 min to detach the pollen-derived micromotors. The pollen-derived micromotors were collected via centrifugation at 6000*g* for 10 min and removed the supernatant. The micromotors were stored in a vacuum environment to reduce oxidation of the magnesium layer.

4.4. Test of motion performance

The pollen-derived micromotors were exposed to artificial gastric juice with different pH value and their motion performance was recorded by a CCD camera.

4.5. Test of retention property in vitro

To test the retention property of pollen-derived micromotors *in vitro*, stomach tissue of mice was employed. The pollen-derived micromotors were dyed with red dyes. Spherical particles with the same size as pollen-derived micromotors were utilized and dyed with black dyes. PBS flows with the same amount of pollen-derived micromotors and spherical particles were arranged to flush through the stomach tissue, respectively. The amount of particles remained on the stomach tissue was counted for calculating the initial retention ratio. After that, fresh pure PBS flows were employed to flush the stomach tissue twice. Then, a second counting was carried out to calculate the retention rate after flushing.

4.6. Test of retention property in vivo

To test the retention property of pollen-derived micromotors *in vivo*, mice were randomly divided into four groups. These four groups received gavage of PBS, spherical microparticles, SECs and pollen-derived micromotors, respectively. Notably, all the particles were dyed with Rhodamine B to endow them with fluorescence signal. Then, they were sacrificed on specific time points and their digestive tracts were taken out for analysis of fluorescence retention.

4.7. Test of drug loading and drug release

Rhodamine B was utilized as drug model in this experiment to test the drug loading and drug release capacity. Rhodamine B was loaded into the SECs by simply immersing SECs in the aqueous solution of Rhodamine B, followed by vacuum treating. After 12 h, the drug-loaded SECs were centrifugated at 6000 g for 10 min and collected by removing the supernatant. The drug loading (DL) efficiency was calculated via the equation:

$$\text{DL efficiency } (\%) = \frac{mass\ of\ loaded\ drug}{mass\ of\ the\ drug - loaded\ micromotors} * 100\%$$

To observe their drug release kinetics, drug-loaded SECs were exposed to artificial gastric juice. The mixture was oscillated at 400 rpm at 37 °C. Then, we took out the supernatants at specific time interval into a 96-well plate, followed by supplying equal volume of fresh artificial gastric juice to the mixture. By scanning the 96-well plate with the help of microplate reader at 488 nm, the data was collected for calculation of the cumulative release rate.

4.8. Test of hemolysis of pollen-derived micromotors

To test their hemolysis, we took the blood sample from mouse and collected it in an anticoagulant tube. Then, the red blood cell was purified by centrifugating the blood sample at 1500 rpm for 5 min for 10 times. Then, normal saline was used to adjust the cell concentration to a value of 2 v/v%. And the new blood solution was divided equally into three groups. Then, normal saline, DI water and pollen-derived micromotors were added to the three groups, respectively, serving as negative control group, positive control group and experimental group. After 3 h, the supernatant of three groups were sucked out to measure OD value at 570 nm. The calculation formulation of hemolysis was demonstrated in Fig. S9.

4.9. Test of biocompatibility of pollen-derived micromotors

NIH-3T3 cells were cultured for the test of biocompatibility of pollen-derived micromotors. Cells were cultured according to our previous work [46]. We set three groups in this manuscript, which involve control group, pollen group and micromotor group. First, same amount of culture medium and NIH-3T3 cells were added to a single well of the 6-well plate. Then, the pollens and micromotors were soaked into the culture medium with the help of sieves, as shown in Fig. S10a. After cells were cultured for 24 h, MTT solution was added to the culture medium. After 4 h, sieves containing materials were removed, followed by adding dimethyl sulfoxide to the culture medium. Then, same amount of culture medium of each group was collected for measuring the OD value. To calculate the relative activity, the OD value of control group each day was set as 100%. On day 3, the cells were imaged by using calcein AM to stain them. The cell images were captured by fluorescence microscope after washing cells with PBS for three times.

4.10. Gastric ulcer model establishment of mice

To establish the gastric ulcer model, the mice were fasted overnight. Then, mice were given a gavage of DI water (0.5 mL). Repeated the gavage after 3 h. After 2 h, the mice were given acetic acid aqueous solution (20 v/v%) by gavage, whose volume corresponds to their weight (0.025 mL/10 g). All animal experiments were approved by Animal Investigation Ethics Committee of Drum Tower Hospital.

4.11. Test of the therapeutic efficacy of pollen-derived micromotors on gastric ulcer

To demonstrate the therapeutic efficacy of pollen-derived micromotors on gastric ulcer, berberine hydrochloride, an extract of Chinese herb coptis chinensis, was chosen as the drug. We firstly divided mice into four groups at random. One group of them was set as healthy control group and the other three were established with gastric ulcer model on Day 0. The healthy group received gavage of PBS while the other three groups received gavage of PBS, free berberine hydrochloride dissolved in PBS, and berberine hydrochloride-loaded micromotors dispersed in PBS, respectively. Notably, all mice were fasted overnight before every gavage to empty chyme in the stomach, which would benefit the adherence of micromotors to the stomach wall. Gavage was carried out on Day 1, Day 3 and Day 5. And on Day 7, all the mice were sacrificed and their stomach tissues were taken out for histopathological analysis. Also, the weight of mice was recorded on Day 0, Day 1, 3, 5, and 7.

Ethics

All animal experiments were approved by Animal Investigation Ethics Committee of Drum Tower Hospital. (2019AE01012).

CRediT authorship contribution statement

Lijun Cai: Methodology, Investigation, Writing – original draft, Validation, Formal analysis. **Cheng Zhao:** Validation, Formal analysis. **Xinyue Cao:** Writing – review & editing. **Minhui Lu:** Writing – review & editing. **Ning Li:** Writing – review & editing. **Yuan Luo:** Writing – review & editing, Resources. **Yongan Wang:** Writing – review & editing, Resources. **Yuanjin Zhao:** Conceptualization, Methodology, Supervision, Resources.

Declaration of competing interest

The authors declare that they have no known competing financial interests or personal relationships that could have appeared to influence the work reported in this paper.

Acknowledgement

This work was supported by the National Key Research and Development Program of China (2022YFA1105300), the National Natural Science Foundation of China (T2225003, 52073060 and 61927805), the Nanjing Medical Science and Technique Development Foundation (ZKX21019), the Clinical Trials from Nanjing Drum Tower Hospital (2022-LCYJ-ZD-01), Guangdong Basic and Applied Basic Research Foundation (2021B1515120054), and the Shenzhen Fundamental Research Program (JCYJ20190813152616459 and JCYJ20210324133214038).

Appendix A. Supplementary data

Supplementary data to this article can be found online at https://doi.org/10.1016/j.bioactmat.2023.09.009.

References

[1] E.X.Z. Tan, S. Hui, K. Asadi, D. Wong, Searching for a cause of a gastric ulcer in case of common variable immunodeficiency: cytomegalovirus, Lancet 400 (10361) (2022) 1437.
[2] K.W. McCracken, E.M. Catá, C.M. Crawford, K.L. Sinagoga, M. Schumacher, B. E. Rockich, Y. Tsai, Christopher N. Mayhew, Jason R. Spence, Yana Zavros, James M. Wells, Modelling human development and disease in pluripotent stem-cell-derived gastric organoids, Nature 516 (2014) 400–404.
[3] Y. Dong, L. Wang, N. Xia, Z. Yang, C. Zhang, C. Pan, D. Jin, J. Zhang, C. Majidi, L. Zhang, Untethered small-scale magnetic soft robot with programmable magnetization and integrated multifunctional modules, Sci. Adv. 8 (25) (2022), eabn8932.
[4] K. Shitara, J.A. Ajani, M. Moehler, M. Garrido, C. Gallardo, L. Shen, K. Yamaguchi, L. Wyrwicz, T. Skoczylas, A.C. Bragagnoli, T. Liu, M. Tehfe, E. Elimova, R. Bruges, T. Zander, S. de Azevedo, R. Kowalyszyn, R. Pazo-Cid, M. Schenker, J.M. Cleary, P. Yanez, K. Feeney, M.V. Karamouzis, V. Poulart, M. Lei, H. Xiao, K. Kondo, M. Li, Y.Y. Janjigian, Nivolumab plus chemotherapy or ipilimumab in gastro-oesophageal cancer, Nature 603 (2022) 942–948.
[5] X. Xu, X. Xia, K. Zhang, A. Rai, Z. Li, P. Zhao, K. Wei, L. Zou, B. Yang, W. Wong, P. W. Chiu, L. Bian, Bioadhesive hydrogels demonstrating pH-independent and ultrafast gelation promote gastric ulcer healing in pigs, Sci. Transl. Med. 12 (558) (2020), eaba8014.
[6] W. Zhang, Y. Zhou, Y. Fan, R. Cao, Y. Xu, Z. Weng, J. Ye, C. He, Y. Zhu, X. Wang, Metal-organic-framework-Based hydrogen-release platform for multieffective Helicobacter pylori targeting therapy and intestinal flora protective capabilities, Adv. Mater. 34 (2) (2022), 2105738.
[7] Q. Wang, Y. Xu, R. Xue, J. Fan, H. Yu, J. Guan, H. Wang, M. Li, W. Yu, Z. Xie, R. Qi, X. Jia, B. Han, All-in-One theranostic platform based on hollow microcapsules for intragastric-targeting antiulcer drug delivery, CT imaging, and synergistically healing gastric ulcer, Small 18 (9) (2022), 2104660.
[8] Q. Saiding, Z. Cai, L. Deng, W. Cui, Inflammation self-limiting electrospun fibrous tape via regional immunity for deep soft tissue repair, Small 18 (39) (2022), 2203265.
[9] J. Chen, J.S. Caserto, I. Ang, K. Shariati, J. Webb, B. Wang, X. Wang, N. Bouklas, M. Ma, An adhesive and resilient hydrogel for the sealing and treatment of gastric perforation, Bioact. Mater. 14 (2022) 52–60.
[10] W. Huang, R. Chen, Y. Peng, F. Duan, Y. Huang, W. Guo, X. Chen, L. Nie, In vivo quantitative photoacoustic diagnosis of gastric and intestinal dysfunctions with a broad pH-responsive sensor, ACS Nano 13 (8) (2019) 9561–9570.
[11] M.M. Ali, M. Wolfe, K. Tram, J. Gu, C.D.M. Filipe, Y. Li, J.D. Brennan, A DNAzyme-based colorimetric paper sensor for Helicobacter pylori, Angew. Chem. Int. Ed. 58 (29) (2019) 9907–9911.
[12] R. Cheng, L. Liu, Y. Xiang, Y. Lu, L. Deng, H. Zhang, H.A. Santos, W. Cui, Advanced liposome-loaded scaffolds for therapeutic and tissue engineering applications, Biomaterials 232 (2020), 119706.
[13] A. Abramson, E. Caffarel-Salvador, M. Khang, D. Dellal, D. Silverstein, Y. Gao, M. R. Frederiksen, A. Vegge, F. Hubálek, J.J. Water, A.V. Friderichsen, J. Fels, R. K. Kirk, C. Cleveland, J. Collins, S. Tamang, A. Hayward, T. Landh, S.T. Buckley, N. Roxhed, U. Rahbek, R. Langer, G. Traverso, An ingestible self-orienting system for oral delivery of macromolecules, Science 363 (6427) (2019) 611–615.
[14] L. Cai, C. Zhao, H. Chen, L. Fan, Y. Zhao, X. Qian, R. Chai, Suction-cup-inspired adhesive micromotors for drug delivery, Adv. Sci. 9 (1) (2022), 2103384.
[15] Z. Lin, C. Gao, D. Wang, Q. He, Bubble-propelled Janus Gallium/zinc micromotors for the active treatment of bacterial infections, Angew. Chem. Int. Ed. 60 (1) (2021) 1–6.
[16] D.M. Griffith, H. Li, M.V. Werrett, P.C. Andrews, H. Sun, Medicinal chemistry and biomedical applications of bismuth-based compounds and nanoparticles, Chem. Soc. Rev. 50 (2021) 12037–12069.
[17] L. Olbe, E. Carlsson, P. Lindberg, A proton-pump inhibitor expedition: the case histories of omeprazole and esomeprazole, Nat. Rev. Drug Discov. 2 (2003) 132–139.

[18] I. Thung, H. Aramin, V. Vavinskaya, S. Gupta, J.Y. Park, S.E. Crow, M.A. Valasek, Review article: the global emergence of Helicobacter pylori antibiotic resistance, Aliment. Pharmacol. Ther. 43 (4) (2016) 514–533.
[19] G.L.H. Wong, L.H.S. Lau, J.Y.L. Ching, Y. Tse, R.H.Y. Ling, V.W.S. Wong, P.W. Y. Chiu, J.Y.W. Lau, F.K.L. Chan, Prevention of recurrent idiopathic gastroduodenal ulcer bleeding: a double-blind, randomised trial, Gut 69 (4) (2020) 652–657.
[20] T. Friedemann, M. Li, J. Fei, U. Schumacher, J. Song, S. Schroeder, Hypothesis-driven screening of Chinese herbs for compounds that promote neuroprotection, Science 350 (2015) S69–S71.
[21] S. Tang, L. Yang, Y. Kuroda, S. Lai, S. Xie, H. Zhang, I. Katayama, Herb sanqi-derived compound K alleviates oxidative stress in cultured human melanocytes and improves oxidative-stress-related leukoderma in Guinea pigs, Cells 10 (8) (2021) 2057.
[22] T. Wang, W. Tseng, Y. Leu, C. Chen, W. Lee, Y. Chi, S. Cheng, C. Lai, C. Kuo, S. Yang, S. Yang, J. Shen, C. Feng, C. Wu, T. Hwang, C. Wang, S. Wang, C. Chen, The flavonoid corylin exhibits lifespan extension properties in mouse, Nat. Commun. 13 (2022) 1238.
[23] Z. Chang, W. Qin, H. Zheng, K. Schegg, L. Han, X. Liu, Y. Wang, Z. Wang, H. McSwiggin, H. Peng, S. Yuan, J. Wu, Y. Wang, S. Zhu, Y. Jiang, H. Nie, Y. Tang, Y. Zhou, M.J.M. Hitchcock, Y. Tang, W. Yan, Triptonide is a reversible non-hormonal male contraceptive agent in mice and non-human primates, Nat. Commun. 12 (2021) 1253.
[24] T. Fan, S. Park, Q. Shi, X. Zhang, Q. Liu, Y. Song, H. Chin, M.S.B. Ibrahim, N. Mokrzecka, Y. Yang, H. Li, J. Song, S. Suresh, N. Cho, Transformation of hard pollen into soft matter, Nat. Commun. 11 (2020) 1449.
[25] S. Ourani-Pourdashti, A. Azadi, Pollens in therapeutic/diagnostic systems and immune system targeting, J. Contr. Release 340 (2021) 308–317.
[26] S. Iravani, R.S. Varma, Plant pollen grains: a move towards green drug and vaccine delivery system, Nano-Micro Lett. 13 (2021) 128.
[27] T. Yong, X. Zhang, N. Bie, H. Zhang, X. Zhang, F. Li, A. Hakeem, J. Hu, L. Gan, H. A. Santos, X. Yang, Tumor exosome-based nanoparticles are efficient drug carriers for chemotherapy, Nat. Commun. 10 (2019) 3838.
[28] C.C. Mayorga-Martinez, M. Fojtů, J. Vyskočil, N. Cho, M. Pumera, Pollen-Based magnetic microrobots are mediated by electrostatic forces to attract, manipulate, and kill cancer cells, Adv. Funct. Mater. 32 (46) (2022), 2207272.
[29] X. Shou, Y. Yu, D. Wu, F. Wang, W. Sun, P. Duan, L. Shang, Spiny pollen-based antigen-presenting clusters for promoting T cells expansion, Chem. Eng. J. 437 (1) (2022), 135374.
[30] K. Stamatopoulos, V. Kafourou, H.K. Batchelor, S.J. Konteles, Sporopollenin exine microcapsules as potential intestinal delivery system of probiotics, Small 17 (7) (2021), 2004573.
[31] H. Wang, M.G. Potroz, J.A. Jackman, B. Khezri, T. Maric, N. Cho, M. Pumera, Bioinspired spiky micromotors based on sporopollenin exine capsules, Adv. Funct. Mater. 27 (32) (2017), 1702338.
[32] J. Zhang, L. Zeng, Z. Qiao, J. Wang, X. Jiang, Y.S. Zhang, H. Yang, Functionalizing double-network hydrogels for applications in remote actuation and in low-temperature strain sensing, ACS Appl. Mater. Interfaces 12 (27) (2020) 30247–30258.
[33] L. Cai, H. Wang, Y. Yu, F. Bian, Y. Wang, K. Shi, F. Ye, Y. Zhao, Stomatocyte structural color-barcode micromotors for multiplex assays, Natl. Sci. Rev. 7 (3) (2020) 644–651.
[34] M. Qin, M. Sun, M. Hua, X. He, Bioinspired structural color sensors based on responsive soft materials, Curr. Opin. Solid. St. M. 23 (1) (2019) 13–27.
[35] Y. Yan, Y. Zhao, Y. Alsaid, B. Yao, Y. Zhang, S. Wu, X. He, Artificial phototropic systems for enhanced light harvesting based on a liquid crystal elastomer, Adv. Intell. Syst. 3 (10) (2021), 2000234.
[36] G. Xie, J. Forth, S. Zhu, B.A. Helms, P.D. Ashby, H.C. Shum, T.P. Russell, Hanging droplets from liquid surfaces, Proc. Natl. Acad. Sci. U.S.A. 117 (25) (2020) 8360–8365.
[37] L. Cai, D. Xu, H. Chen, L. Wang, Y. Zhao, Designing bioactive micro-/nanomotors for engineered regeneration, Eng. Regen. 2 (2021) 109–115.
[38] C. Gao, Y. Wang, Z. Ye, Z. Lin, X. Ma, Q. He, Biomedical micro-/nanomotors: from overcoming biological barriers to in vivo imaging, Adv. Mater. 33 (6) (2021), 2000512.
[39] L. Cai, N. Li, Y. Zhang, H. Gu, Y. Zhu, Microfluidics-derived microcarrier systems for oral delivery, Biomed. Technol. 1 (2023) 30–38.
[40] B. Ávila, P. Angsantikul, J. Li, M. Lopez-Ramirez, D. Ramírez-Herrera, S. Thamphiwatana, C. Chen, J. Delezuk, R. Samakapiruk, V. Ramez, M. Obonyo, L. Zhang, J. Wang, Micromotor-enabled active drug delivery for in vivo treatment of stomach infection, Nat. Commun. 8 (2017) 272.
[41] Z. Wu, L. Li, Y. Yang, P. Hu, Y. Li, S. Yang, L. Wang, W. Gao, A microrobotic system guided by photoacoustic computed tomography for targeted navigation in intestines in vivo, Sci. Robot. 4 (2019), eaax0613.
[42] T. Li, S. Yu, B. Sun, Y. Li, X. Wang, Y. Pan, C. Song, Y. Ren, Z. Zhang, K. Grattan, Z. Wu, J. Zhao, Bioinspired claw-engaged and biolubricated swimming microrobots creating active retention in blood vessels, Sci. Adv. 9 (2023), eadg4501.
[43] Y. Xiao, Z. Tang, J. Wang, C. Liu, N. Kong, O.C. Farokhzad, W. Tao, Oral insulin delivery platforms: strategies to address the biological barriers, Angew. Chem. Int. Ed. 59 (45) (2020) 19787–19795.
[44] E. Kaffash, M. Shahbazi, H. Hatami, N. Ali, An insight into gastrointestinal macromolecule delivery using physical oral devices, Drug Deliv. Today 27 (8) (2022) 2309–2321.
[45] C. Zhao, L. Cai, M. Nie, L. Shang, Y. Wang, Y. Zhao, Cheerios effect inspired microbubbles as suspended and adhered oral delivery systems, Adv. Sci. 8 (7) (2021), 2004184.
[46] L. Cai, G. Chen, Y. Wang, C. Zhao, L. Shang, Y. Zhao, Boston ivy-inspired disc-like adhesive microparticles for drug delivery, Research 2021 (2021), 9895674.